Supplementary Material for the article

Subtropical Extreme Heatwave Dynamics in the Intermediate-Complexity Atmospheric Model Aeolus 2.0

Sullyandro O. Guimarães[1,2*], Masoud Rostami[1,3], Stefan Petri[1]

[1]Potsdam Institute for Climate Impact Research (PIK), Member of the Leibniz Association, Potsdam, Germany
[2]University of Potsdam, Potsdam, Germany
[3]Laboratoire de Météorologie Dynamique (LMD), Sorbonne University (SU), Ecole Normale Supérieure (ENS), Paris, France

[*]Corresponding author, sullyandro@pik-potsdam.de

This document contains supplementary information and figures

November 16, 2025

Model Configuration

The Aeolus 2.0 Stand-alone atmospheric model was configured following similar approach as Rostami et al. (2024; 2025).

The grid used is regular with 384 latitudes by 768 longitudes (~0.5 degrees), passed to Dedalus in a Cartesian domain, to then be processed into Spectral domain using Fourier series. The frequency is every 1 minute (numerical time-step), outputted 4 times per day.

The simulation was performed under 16 cores and 16 GB ram, running for 102 numerical-days (4x per day = 408 time-steps), spending approximately 3hs to complete, for each case studied. The output size by case is 20 GB.

Dedalus framework details are found in Rostami et al. (2024) and in Dedalus Project homepage (dedalus-project.org, Burns et al., 2020). We used Dedalus version 2.2207.3, running in Python 3.10.14.

Other libraries used: Climlab (0.8.2), C-Extensions for Python (cython 3.0.10), NumPy (1.26.4), Scipy (1.13.1), MPI for Python (mpi4py 3.1.6), and HDF5 for Python (h5py 3.11.0).

By enabling high-performance and efficient execution, this framework supplies Dedalus with the essential functionality required for advanced scientific computations.

Simulations were performed in a computer Alienware M18 R1, Processor i9-13900HX (32 Threads, 24 cores, 36 MB L3-Cache, 5.4GHz), 32GB RAM DDR5 4.800MHz (2x16GB), with operational system Ubuntu 22.04.4 LTS.

Aeolus 2.0 Additional Equations in Flux form

Aeolus 2.0 model numerical scheme is presented in a recent approach as a novel flux-globalization-based, well-balanced (WB) path-conservative central-upwind (PCCU), on developments studied by Cao et al. (2025). This innovative approach has led to substantial progress in numerically handling hyperbolic systems that involve nonconservative products. Thanks to this methodology, the TRSW model can now be implemented in a way that ensures both practical usability and high simulation accuracy.

In this new scheme the layers are numbered from the top to bottom, so here the lower layer is index 2 and the upper layer is 1.

The system of governing equations of the two-layer mcTRSW model departure from the following.

$$(\boldsymbol{v}_1)_t + \boldsymbol{v_1} \cdot \boldsymbol{\nabla} \boldsymbol{v}_1 + f\hat{\boldsymbol{z}} \wedge \boldsymbol{v}_1 = -\left(b_1 \boldsymbol{\nabla}(h_1 + Z) + b_2 \boldsymbol{\nabla} h_2 + \frac{1}{2} h_1 \boldsymbol{\nabla} b_1 + h_2 \boldsymbol{\nabla} b_2\right) + \frac{\boldsymbol{v}_2 - \boldsymbol{v}_1}{h_1 b_1} \gamma (C - D) \tag{1}$$

$$(\boldsymbol{v}_2)_t + \boldsymbol{v}_2 \cdot \boldsymbol{\nabla} \boldsymbol{v}_2 + f\hat{\boldsymbol{z}} \wedge \boldsymbol{v}_2 = -\left(b_2 \boldsymbol{\nabla} h_1 + b_2 \boldsymbol{\nabla}(h_2 + Z) + \frac{1}{2} h_2 \boldsymbol{\nabla} b_2\right) \tag{2}$$

$$(h_1)_t + \boldsymbol{\nabla} \cdot (h_1 \boldsymbol{v}_1) = \frac{\gamma (C - D)}{b_1} \tag{3}$$

$$(h_2)_t + \boldsymbol{\nabla} \cdot (h_2 \boldsymbol{v}_2) = -\frac{\gamma (C - D)}{b_2} \tag{4}$$

$$(b_1)_t + \boldsymbol{v}_1 \cdot \boldsymbol{\nabla} b_1 = -\frac{(C - D)}{h_1} \tag{5}$$

$$(b_2)_t + \boldsymbol{v}_2 \cdot \boldsymbol{\nabla} b_2 = \frac{(C - \mu E)}{h_2} \tag{6}$$

$$Q_t + \boldsymbol{\nabla} \cdot (Q \boldsymbol{v}_2) = -C + E \tag{7}$$

Where zonal and meridional coordinates are x and y, $(x, y) \in \Omega$, t is time, $\boldsymbol{\nabla} := (\partial/\partial x, \partial/\partial y)$, $\hat{\boldsymbol{z}}$ is the unit vector in vertical direction, $i = 1, 2$ are the layers index counted from the top, $\boldsymbol{v}_i(x, y, t) = (u_i(x, y, t), v_i(x, y, t))^{\mathrm{T}}$ are the horizontal velocities for each layer, $h_i(x, y, t)$ denotes the

thicknesses of the layers, $b_i = g\overline{\theta}_i/\theta_s$ is the layer-averaged buoyancy, $\overline{\theta}_i$ is the vertically-averaged potential temperature in layer i, θ_s represents a reference surface-level potential temperature, and g is the gravitational acceleration, Z is the bottom topography, and $f(y) = f_0 + \beta y$ is the Coriolis parameter with f_0 and β being constants.

Potential temperature (θ) itself is a thermodynamic measure that reflects the temperature a dry air parcel would attain if compressed or expanded adiabatically to a standard pressure level - commonly the surface pressure. It is a conserved quantity under dry adiabatic conditions and is mathematically defined by $\theta = T(P_s/P)^{\mathcal{R}/C_p}$, where T is the current temperature of the parcel, P_s is the reference pressure level, P is the actual pressure of the parcel, $\mathcal{R}$ is the specific gas constant for dry air, and C_p is the specific heat capacity at constant pressure.

The rescaled columnar bulk humidity in the lower layer is Q, and $C = \frac{Q-Q_s}{\tau}\varkappa(Q - Q_s)$ represents condensation, and $E = \alpha\frac{|v_2|}{|(v_2)_{max}|}(Q_s - Q)\varkappa(Q_s - Q)$ is sea surface evaporation, with $\varkappa$ being the Heaviside function, α is an adjustment coefficient. The downward motion is denoted by D, similar to a downdraft in the adiabatic convective process given by $D = \frac{1}{\kappa}\iint C\,dxdy$, where κ is a fraction of Ω, for $0.97Q_s < Q < Q_s$. In this framework, the lower atmospheric layer is considered nearly saturated with water vapor, while the upper layer remains relatively dry. Once the bulk humidity crosses a prescribed saturation threshold, condensation begins. This process acts as a source term in **Equations (3)** and **(6)** and as a sink in **Equations (4)** and **(5)**. The strength of condensation is controlled by the parameter τ. The constant γ regulates the relative influence of heating versus cooling, as well as the role of updraft and downdraft motions. Finally, the parameter $\mu = \frac{\iint C\,dxdy}{\iint E\,dxdy}$ governs the balance between E (the source of moisture in the lower layer) and C.

Alternatively, we can express **Equations (1)-(7)** in a conservative form as follows:

$$(h_1)_t + (h_1u_1)_x + (h_1v_1)_y = \frac{\gamma(C - D)}{b_1} \tag{8}$$

$$(q_1)_t + \left(h_1u_1^2 + \frac{1}{2}b_1h_1^2\right)_x + (h_1u_1v_1)_y = fh_1v_1 - h_1(h_2b_2)_x - h_1b_1Z_x + u_2\frac{\gamma(C - D)}{b_1} \tag{9}$$

$$(p_1)_t + \left(h_1 v_1^2 + \frac{1}{2} b_1 h_1^2\right)_y + (h_1 u_1 v_1)_x = -f h_1 u_1 - h_1 (h_2 b_2)_y - h_1 b_1 Z_y + v_2 \frac{\gamma(C-D)}{b_1} \tag{10}$$

$$(h_1 b_1)_t + (h_1 u_1 b_1)_x + (h_1 v_1 b_1)_y = -\frac{(1-\gamma)(C-D)}{b_1} \tag{11}$$

$$(h_2)_t + (h_2 u_2)_x + (h_2 v_2)_y = -\frac{\gamma(C-D)}{b_2} \tag{12}$$

$$(q_2)_t + \left(h_2 u_2^2 + \frac{1}{2} b_2 h_2^2\right)_x + (h_2 u_2 v_2)_y = f h_2 v_2 - h_2 b_2 (h_1)_x - h_2 b_2 Z_x - u_2 \frac{\gamma(C-D)}{b_2} \tag{13}$$

$$(p_2)_t + \left(h_2 v_2^2 + \frac{1}{2} b_2 h_2^2\right)_y + (h_2 u_2 v_2)_x = -f h_2 u_2 - h_2 b_2 (h_1)_y - h_2 b_2 Z_y - v_2 \frac{\gamma(C-D)}{b_2} \tag{14}$$

$$(h_2 b_2)_t + (h_2 u_2 b_2)_x + (h_2 v_2 b_2)_y = \frac{(1-\gamma)(C-D)}{b_2} + D - \mu E \tag{15}$$

$$Q_t + (Q u_2)_x + (Q v_2)_y = -C + E \tag{16}$$

For the ith layer of the system, the quantities $q_i := h_i u_i$ and $p_i := h_i v_i$ represent the discharges in the x and y directions, respectively.

One of the main challenges in applying TRSW models is the potential loss of hyperbolicity, which can give rise to Kelvin–Helmholtz instabilities, genuine physical phenomena rather than artifacts of numerical approximation. A further difficulty concerns the balance between fluxes and source terms. Reliable schemes must be well-balanced (WB), meaning they should exactly preserve certain physically relevant steady states. Achieving this property is especially demanding in a rotating frame.

In addition, TRSW and mcTRSW systems require accurate representation of sharp features such as hydraulic jumps and fronts, which adds another layer of complexity. The presence of nonconservative products in **Equations (8)-(16)** introduces further difficulties, since these terms cannot be properly defined in the classical distributional sense. Instead, weak solutions must be interpreted as Borel measures (Maso et al., 1995; LeFloch, 2003). To handle this, a path-conservative framework has been proposed (Parés, 2006) and further advanced in subsequent work by Castro et al. (2008; 2017) and Parés (2009). This approach has significantly improved the

treatment of hyperbolic systems with nonconservative terms, making the TRSW framework suitable for realistic and accurate numerical simulations.

These challenges were addressed by adopting the flux-globalized, well-balanced path-conservative central-upwind (PCCU) scheme introduced by Cao et al. (2023; 2024) for the two-layer TRSW equations. This framework was then extended to the moist-convective case by reformulating the mcTRSW system **Equations (8)-(16)** as follows:

$$\boldsymbol{U}_t + \boldsymbol{K}(\boldsymbol{U})_x + \boldsymbol{L}(\boldsymbol{U})_y = \boldsymbol{M}(\boldsymbol{U}) \tag{17}$$

$$\boldsymbol{K}(\boldsymbol{U}) = \boldsymbol{F}(\boldsymbol{U}) - \boldsymbol{R}(\boldsymbol{U}) \tag{18}$$

$$\boldsymbol{R}(\boldsymbol{U}) = \int_{\hat{x}}^{x} \boldsymbol{S}^x \left(\boldsymbol{U}(\xi, y, t), \boldsymbol{U}_\xi(\xi, y, t), \boldsymbol{U}_y(\xi, y, t)\right) d\xi \tag{19}$$

$$\boldsymbol{L}(\boldsymbol{U}) = \boldsymbol{G}(\boldsymbol{U}) - \boldsymbol{R}(\boldsymbol{U}) \tag{20}$$

$$\boldsymbol{R}(\boldsymbol{U}) = \int_{\hat{y}}^{y} \boldsymbol{S}^y \left(\boldsymbol{U}(x, \eta, t), \boldsymbol{U}_x(x, \eta, t), \boldsymbol{U}_\eta(x, \eta, t)\right) d\eta \tag{21}$$

The integral lower limits in **Equations (19)** and **(21)** are arbitrary numbers. $\boldsymbol{U} = (h_1, q_1, p_1, h_1 b_1, h_2, q_2, p_2, h_2 b_2, Q)^\intercal$, $\boldsymbol{K}$ and $\boldsymbol{L}$ are global fluxes following the relations ahead.

$$\boldsymbol{F}(\boldsymbol{U}) = \left(q_1, \frac{q_1^2}{h_1} + \frac{b_1}{2} h_1^2, \frac{q_1 p_1}{h_1}, q_1 b_1, q_2, \frac{q_2^2}{h_2} + \frac{b_2}{2} h_2^2, \frac{q_2 p_2}{h_2}, q_2 b_2, \frac{Q q_2}{h_2}\right)^\intercal \tag{22}$$

$$\boldsymbol{G}(\boldsymbol{U}) = \left(p_1, \frac{q_1 p_1}{h_1}, \frac{p_1^2}{h_1} + \frac{b_1}{2} h_1^2, p_1 b_1, p_2, \frac{q_2 p_2}{h_2}, \frac{p_2^2}{h_2} + \frac{b_2}{2} h_2^2, p_2 b_2, \frac{Q p_2}{h_2}\right)^\intercal \tag{23}$$

$$\boldsymbol{S}^x = (0, f h_1 v_1 - h_1 (h_2 b_2)_x - h_1 b_1 Z_x, 0,0,0, f h_2 v_2 - h_2 b_2 (h_1)_x - h_2 b_2 Z_x, 0,0,0)^\intercal \tag{24}$$

$$\boldsymbol{S}^y = (0, 0, -f h_1 u_1 - h_1 (h_2 b_2)_y - h_1 b_1 Z_y, 0,0,0, -f h_2 u_2 - h_2 b_2 (h_1)_y - h_2 b_2 Z_y, 0,0)^\intercal \tag{25}$$

Thus, the source terms are represented by $\boldsymbol{M}$ as follows, once they were not present in the dry TRSW equations previously.

$$\boldsymbol{M}(\boldsymbol{U}) = \left(\begin{array}{c} \frac{\gamma(C-D)}{b_1}, u_2\frac{\gamma(C-D)}{b_1}, v_2\frac{\gamma(C-D)}{b_1}, -\frac{(1-\gamma)(C-D)}{b_1}, \\ u_2\frac{\gamma(C-D)}{b_2}, -v_2\frac{\gamma(C-D)}{b_2}, \frac{(1-\gamma)(C-D)}{b_2} + D - \mu E, -C + E \end{array} \right)^{\intercal} \tag{26}$$

Supplementary Figures

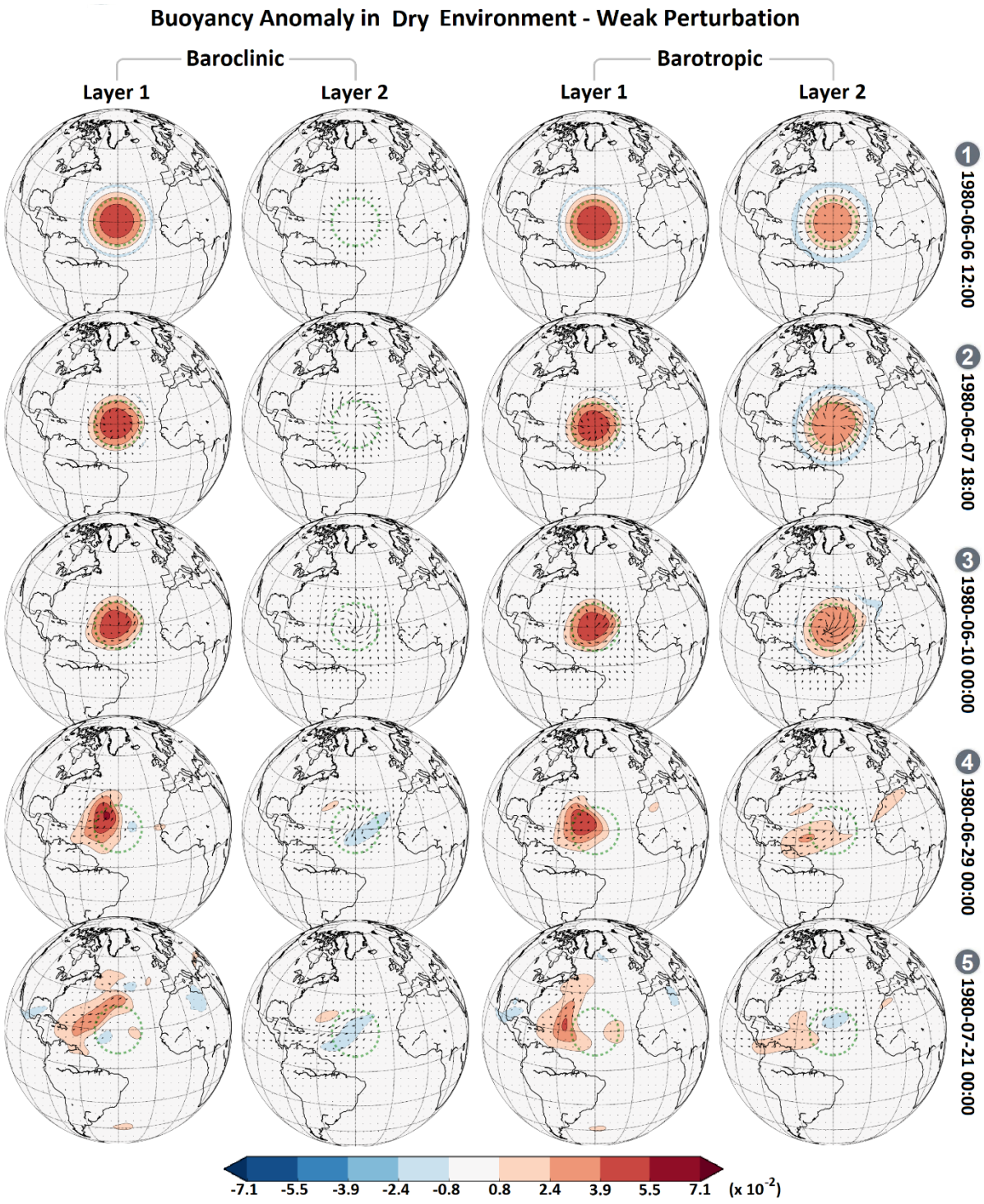

Figure S1: Anomaly evolution of buoyancy by weak perturbation, in the lower (Layer 1) and upper (Layer 2) troposphere, and the corresponding velocity field (represented by arrows) during adjustment in a dry environment, in respect to the reference case. The first and second columns show the results for baroclinic configuration and the third and fourth columns for barotropic. ERA5 data was used as initial condition to startup the model from 1-June-1980.

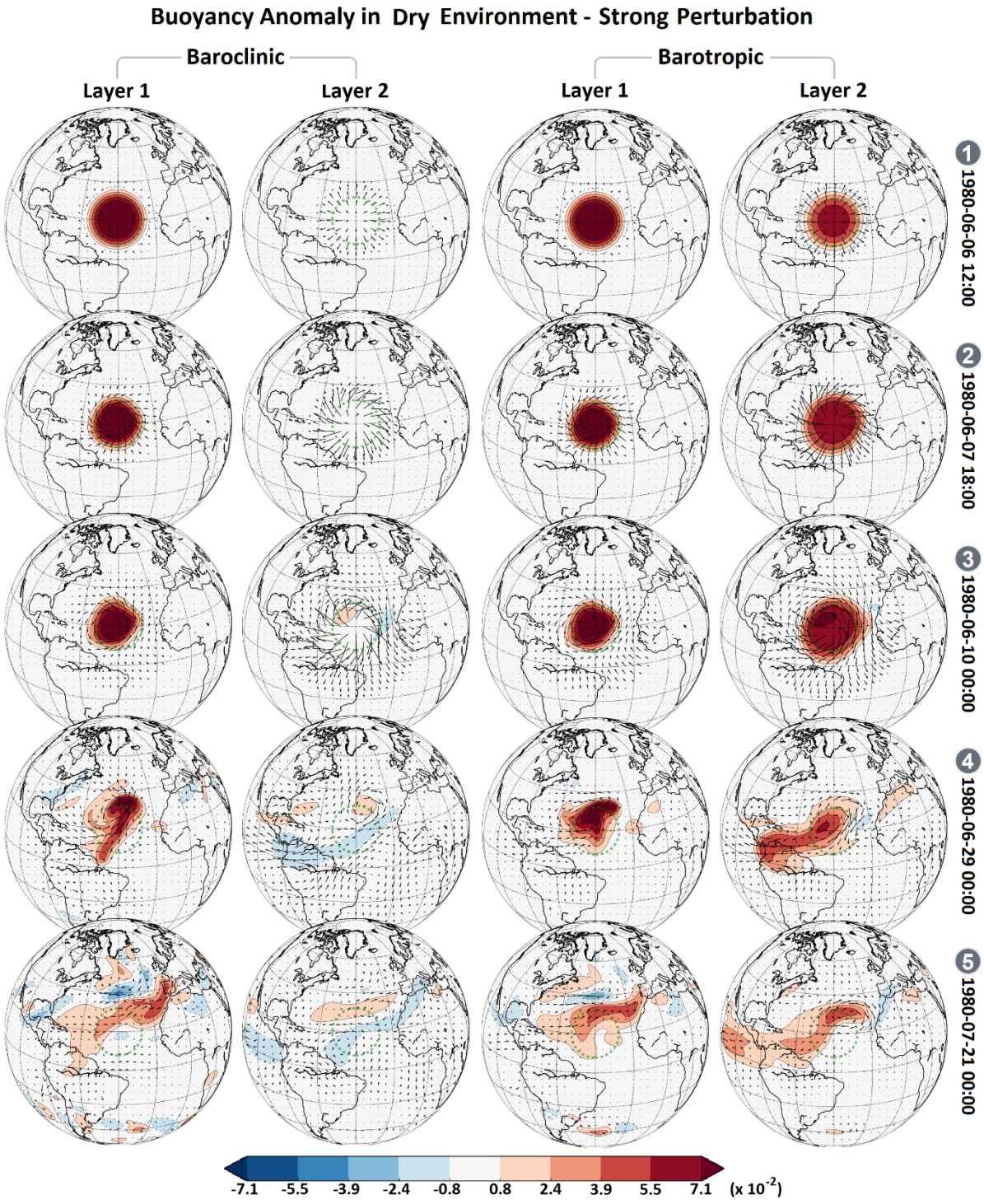

Figure S2: Anomaly evolution of buoyancy by strong perturbation, in the lower (Layer 1) and upper (Layer 2) troposphere, and the corresponding velocity field (represented by arrows) during adjustment in a dry environment, in respect to the reference case. The first and second columns show the results for baroclinic configuration and the third and fourth columns for barotropic. ERA5 data was used as initial condition to startup the model from 1-June-1980.

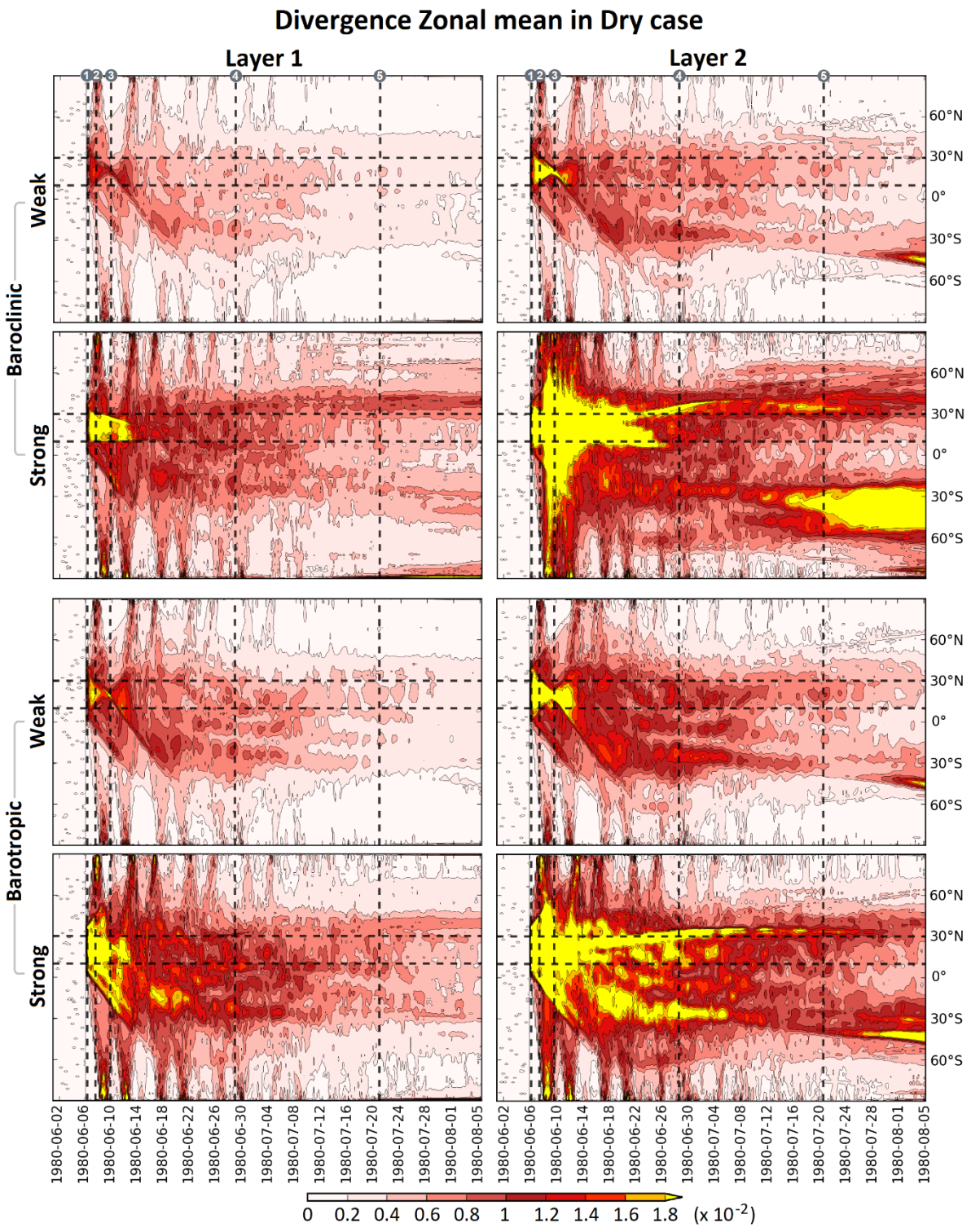

Figure S3: Divergence anomaly zonal mean, relative to the reference case, for dry situations. The horizontal dashed lines represent the initial buoyancy perturbation region. Markers on the top border indicate the time-steps of maps displayed in previous figures.

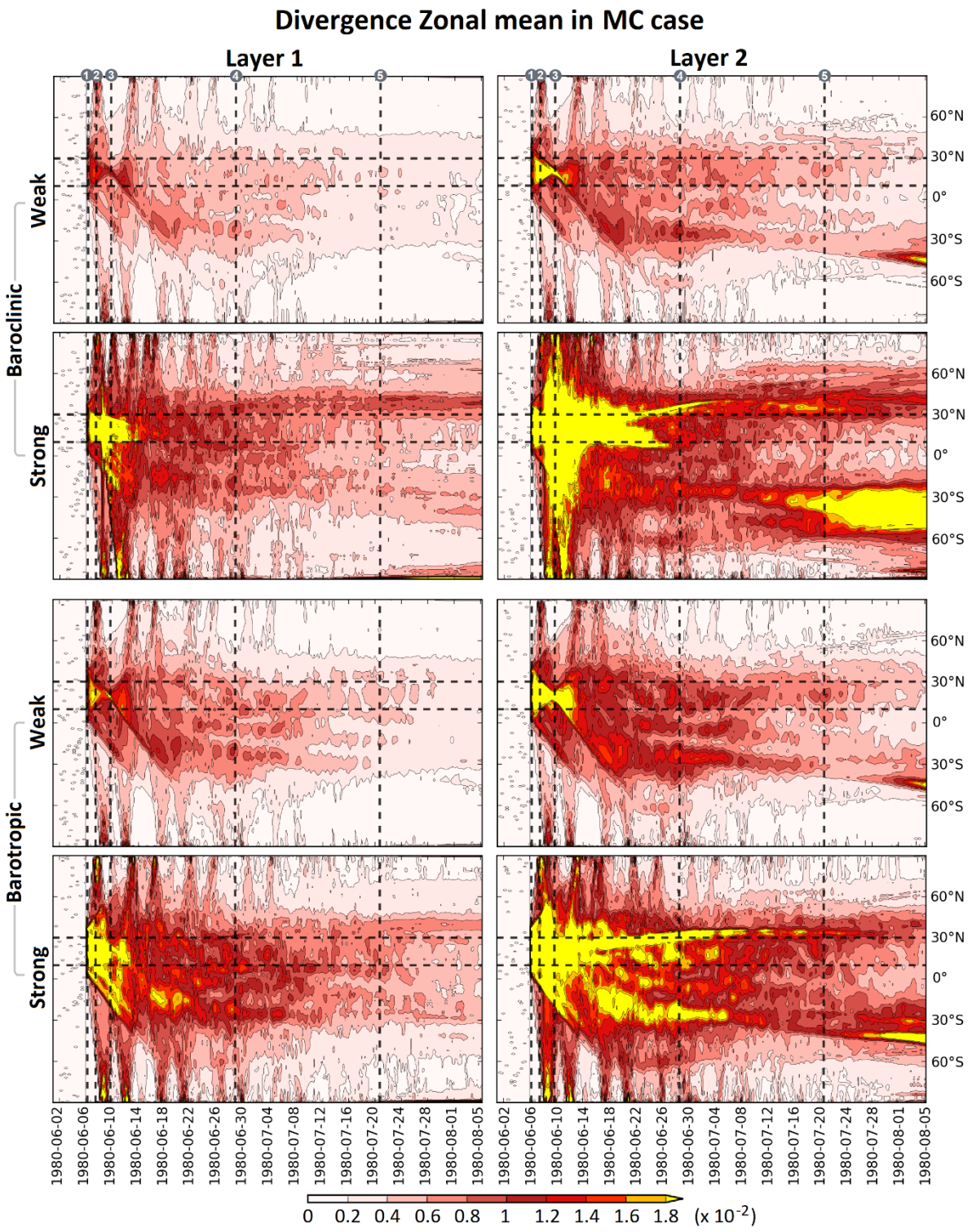

Figure S4: Divergence anomaly zonal mean, relative to the reference case, for moist-convective (MC) situations. The horizontal dashed lines represent the initial buoyancy perturbation region. Markers on the top border indicate the time-steps of maps displayed in previous figures.

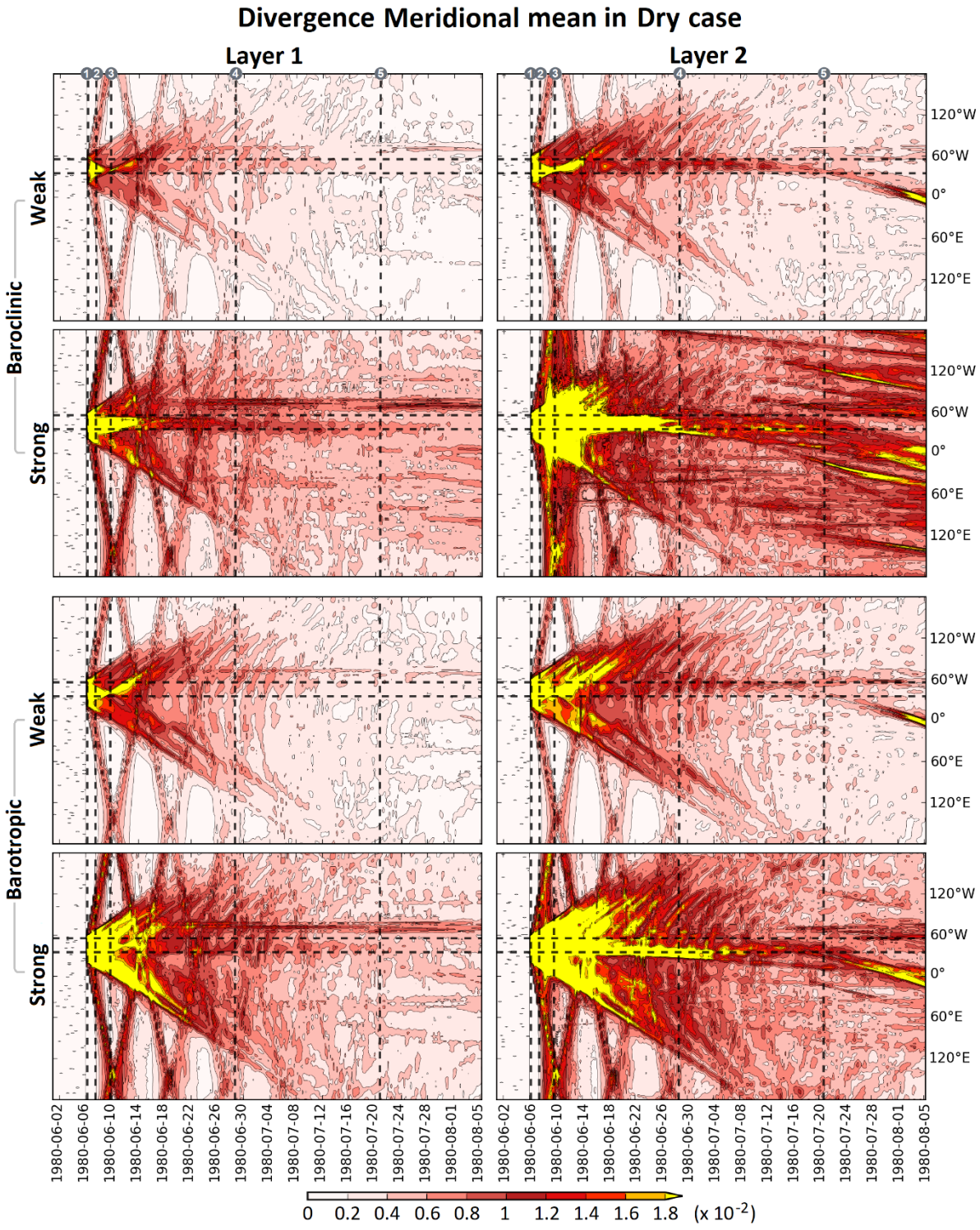

Figure S5: Divergence anomaly meridional mean, relative to the reference case, for dry situations. The horizontal dashed lines represent the initial buoyancy perturbation region. Markers on the top border indicate the time-steps of maps displayed in previous figures.

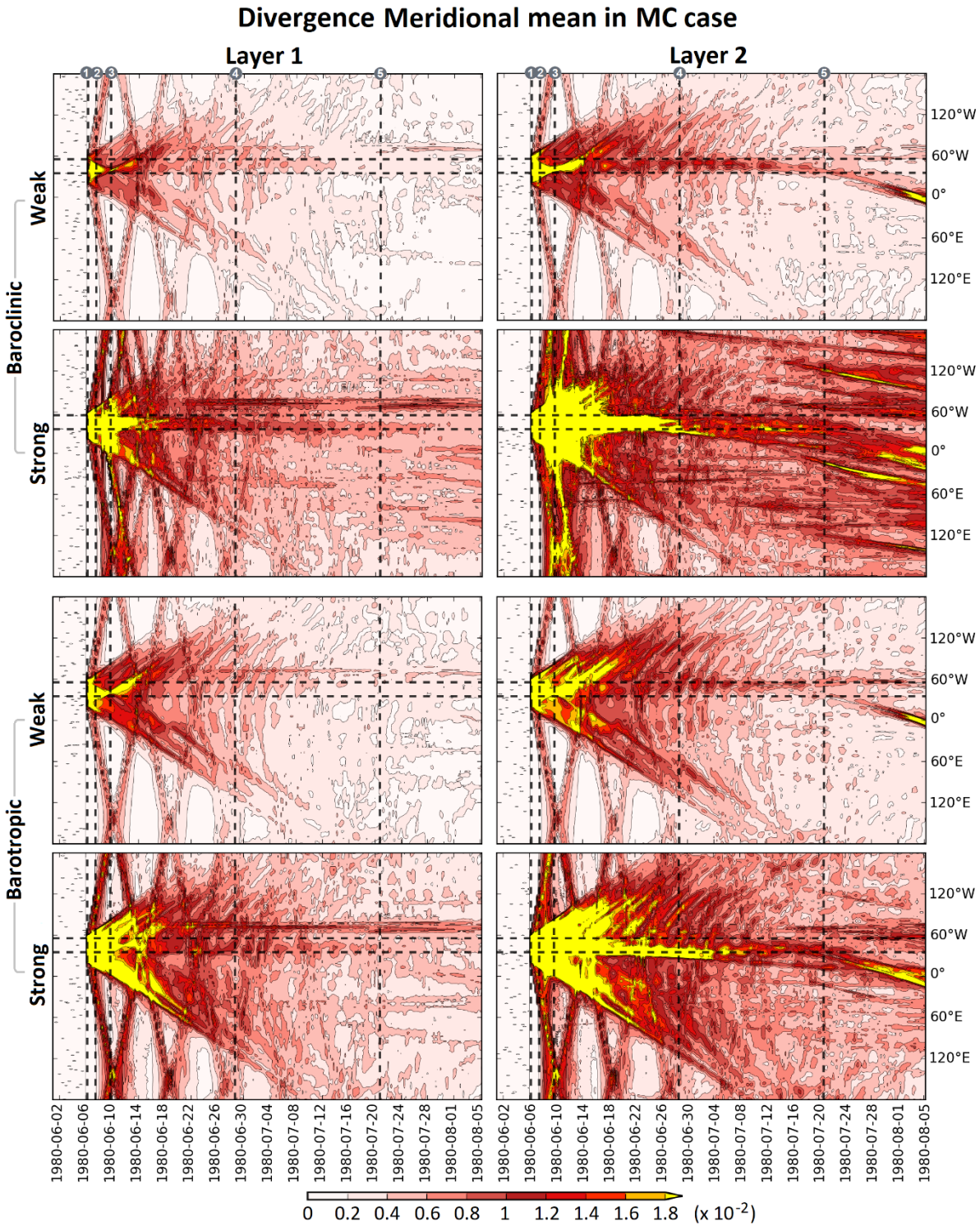

Figure S6: Divergence anomaly meridional mean, relative to the reference case, for moist-convective (MC) situations. The horizontal dashed lines represent the initial buoyancy perturbation region. Markers on the top border indicate the time-steps of maps displayed in previous figures.

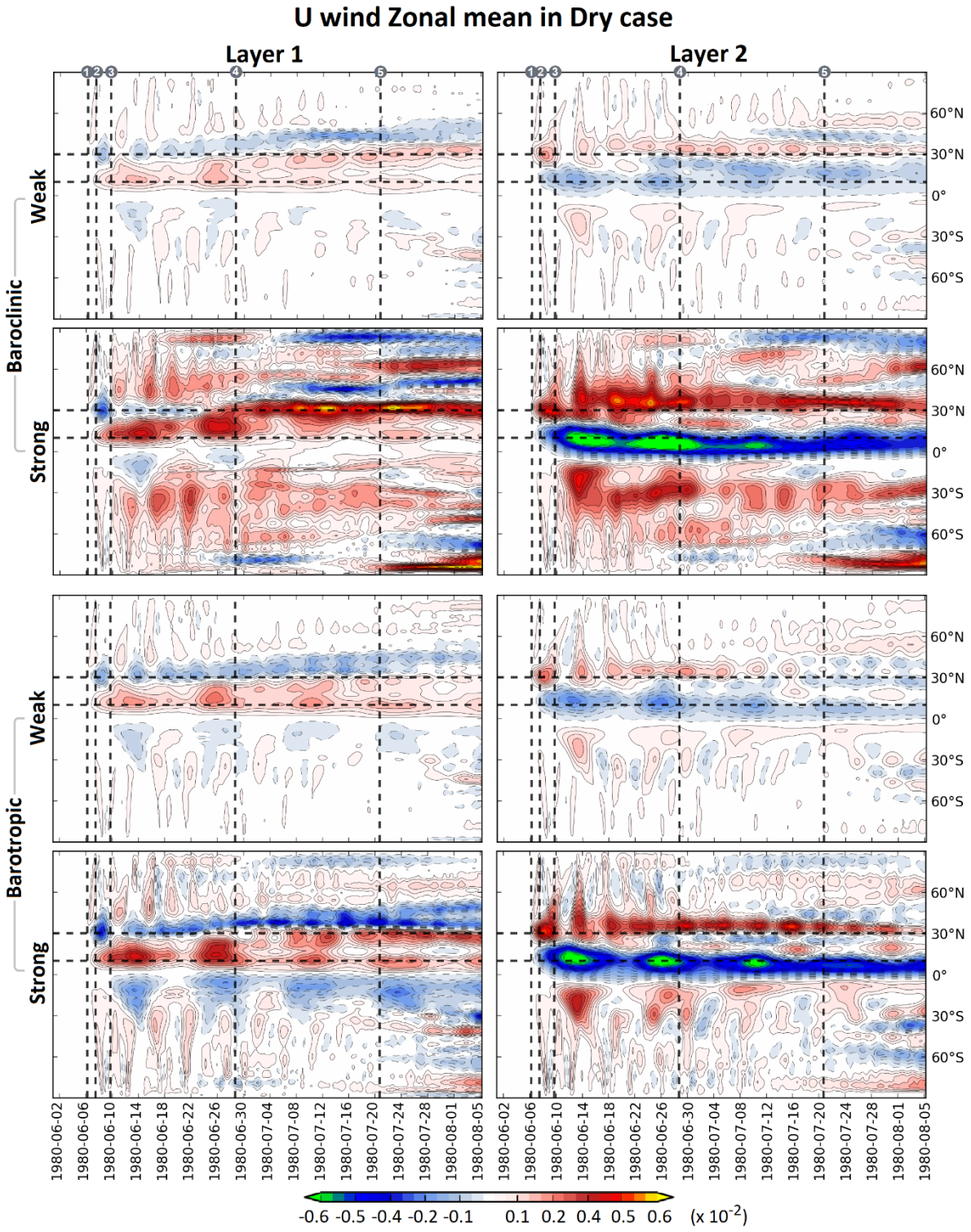

Figure S7: U wind anomaly zonal mean, relative to the reference case, for dry situations. The horizontal dashed lines represent the initial buoyancy perturbation region. Markers on the top border indicate the time-steps of maps displayed in previous figures.

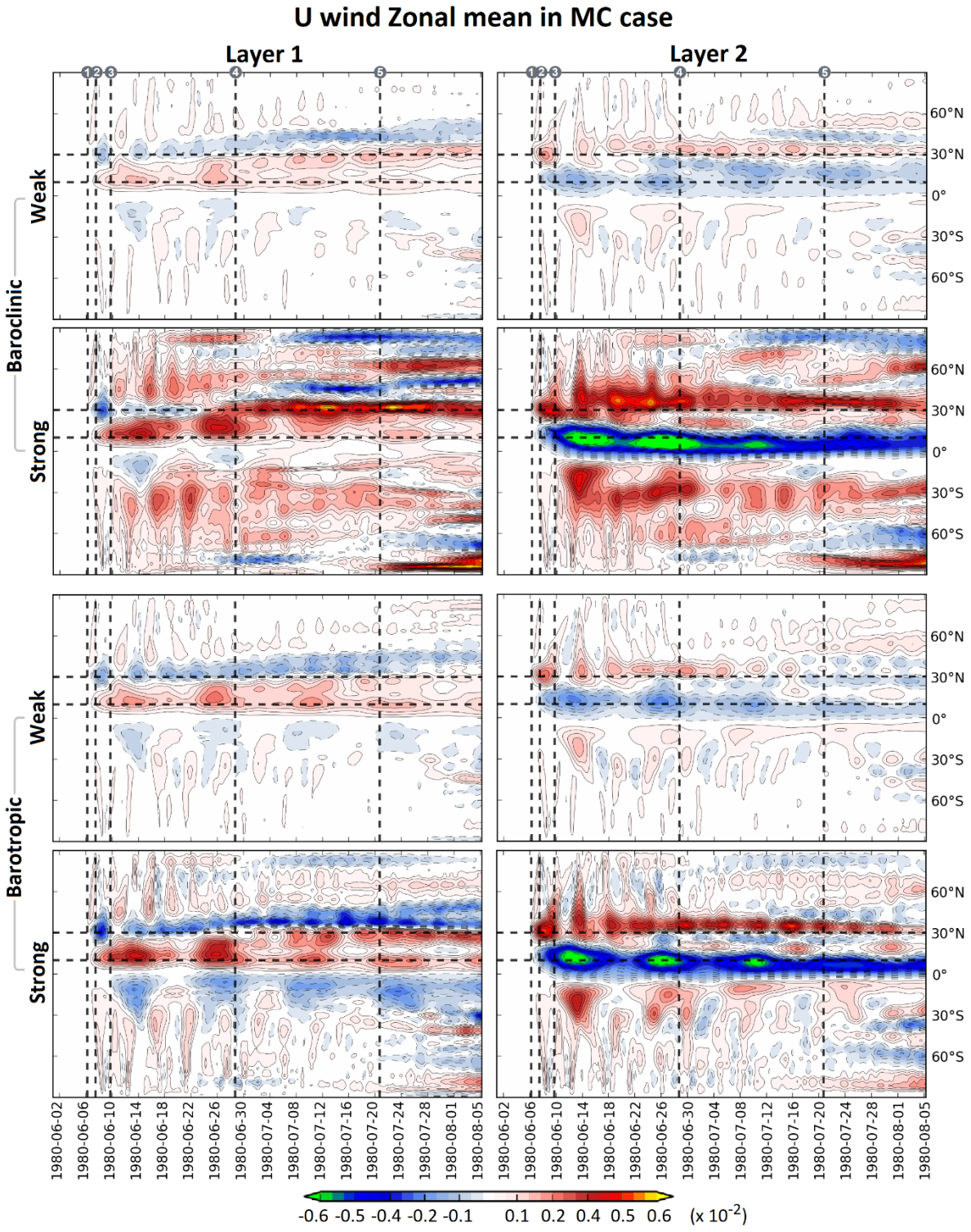

Figure S8: U wind anomaly zonal mean, relative to the reference case, for moist-convective (MC) situations. The horizontal dashed lines represent the initial buoyancy perturbation region. Markers on the top border indicate the time-steps of maps displayed in previous figures.

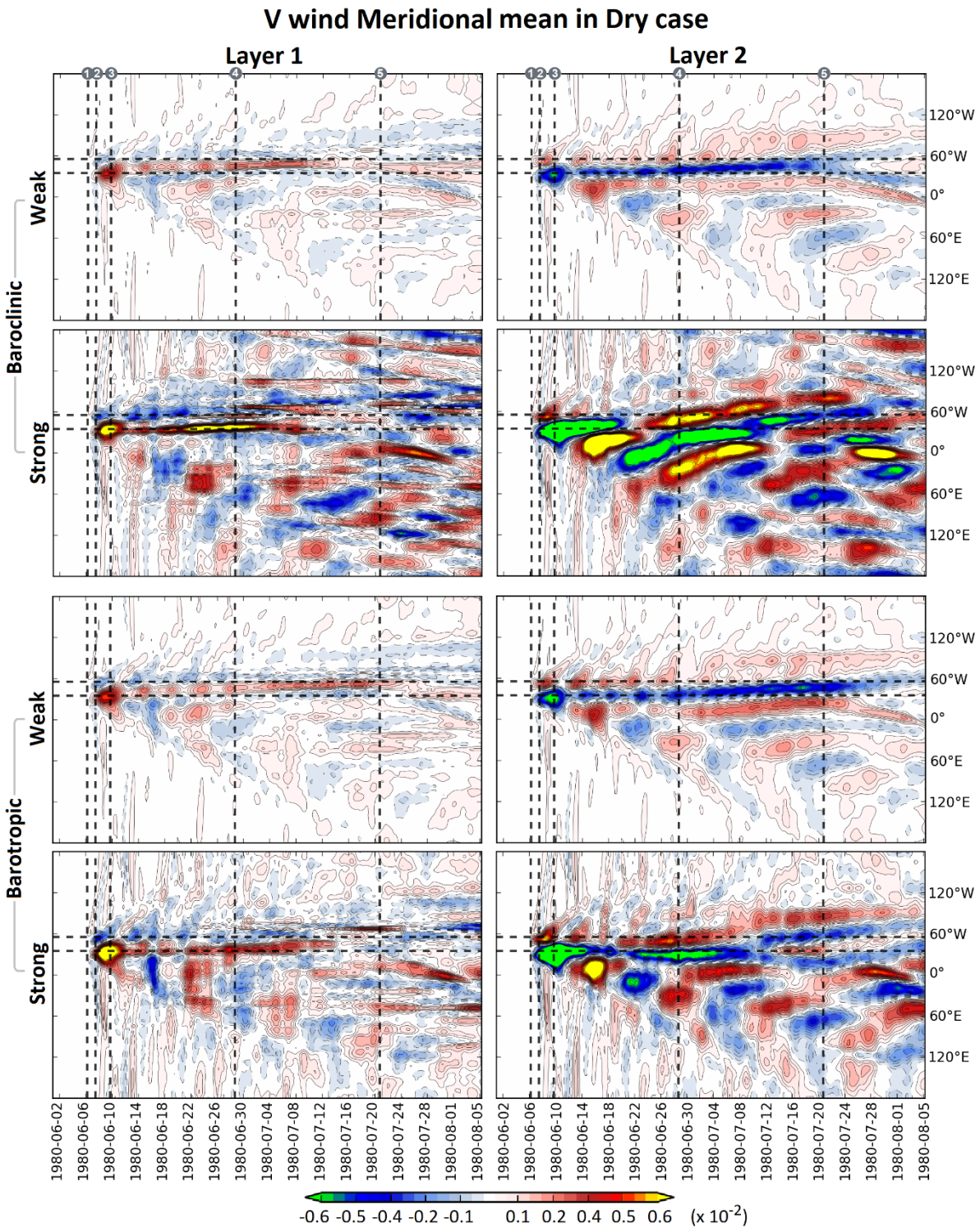

Figure S9: V wind anomaly meridional mean, relative to the reference case, for dry situations. The horizontal dashed lines represent the initial buoyancy perturbation region. Markers on the top border indicate the time-steps of maps displayed in previous figures.

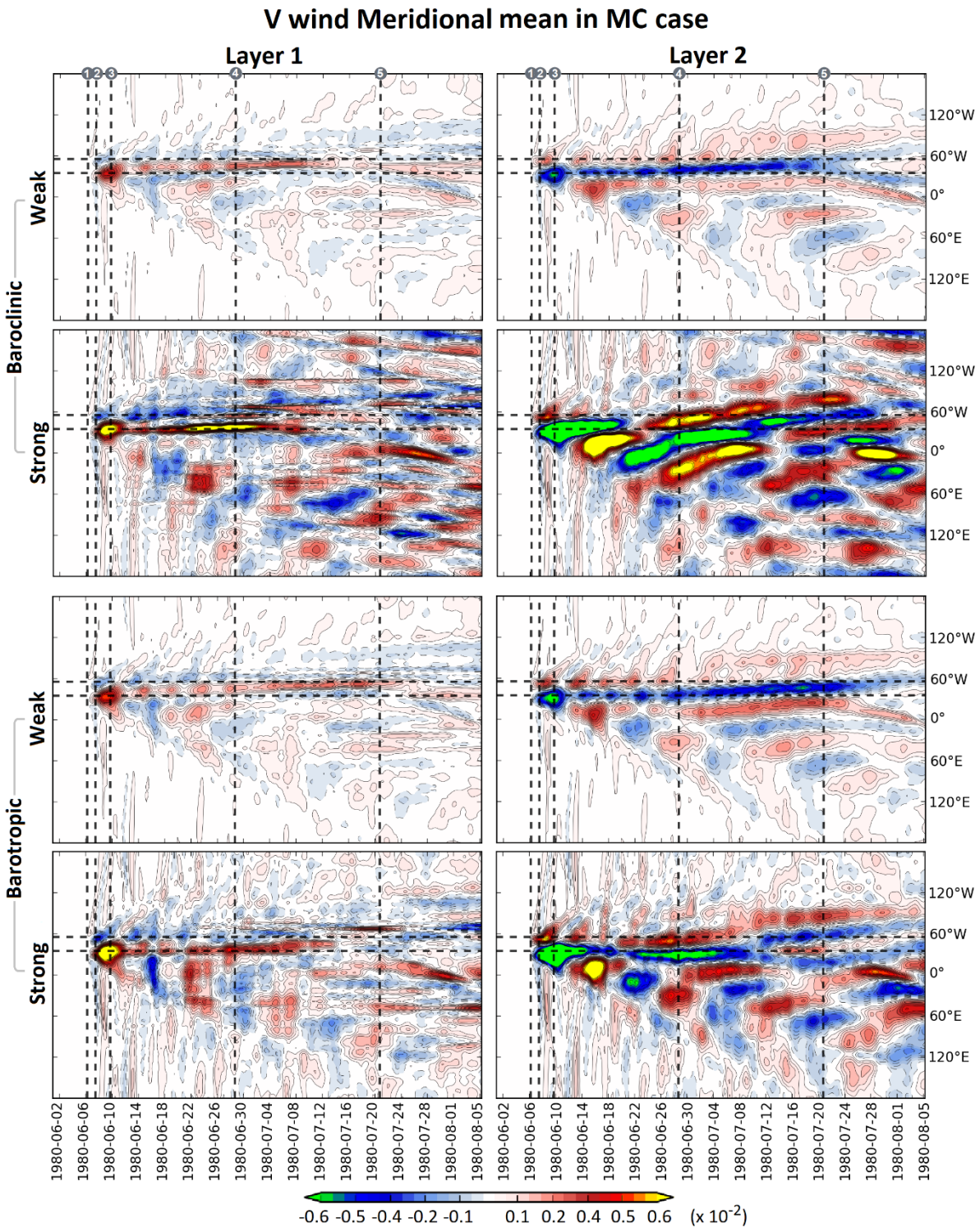

Figure S10: V wind anomaly meridional mean, relative to the reference case, for moist-convective (MC) situations. The horizontal dashed lines represent the initial buoyancy perturbation region. Markers on the top border indicate the time-steps of maps displayed in previous figures.

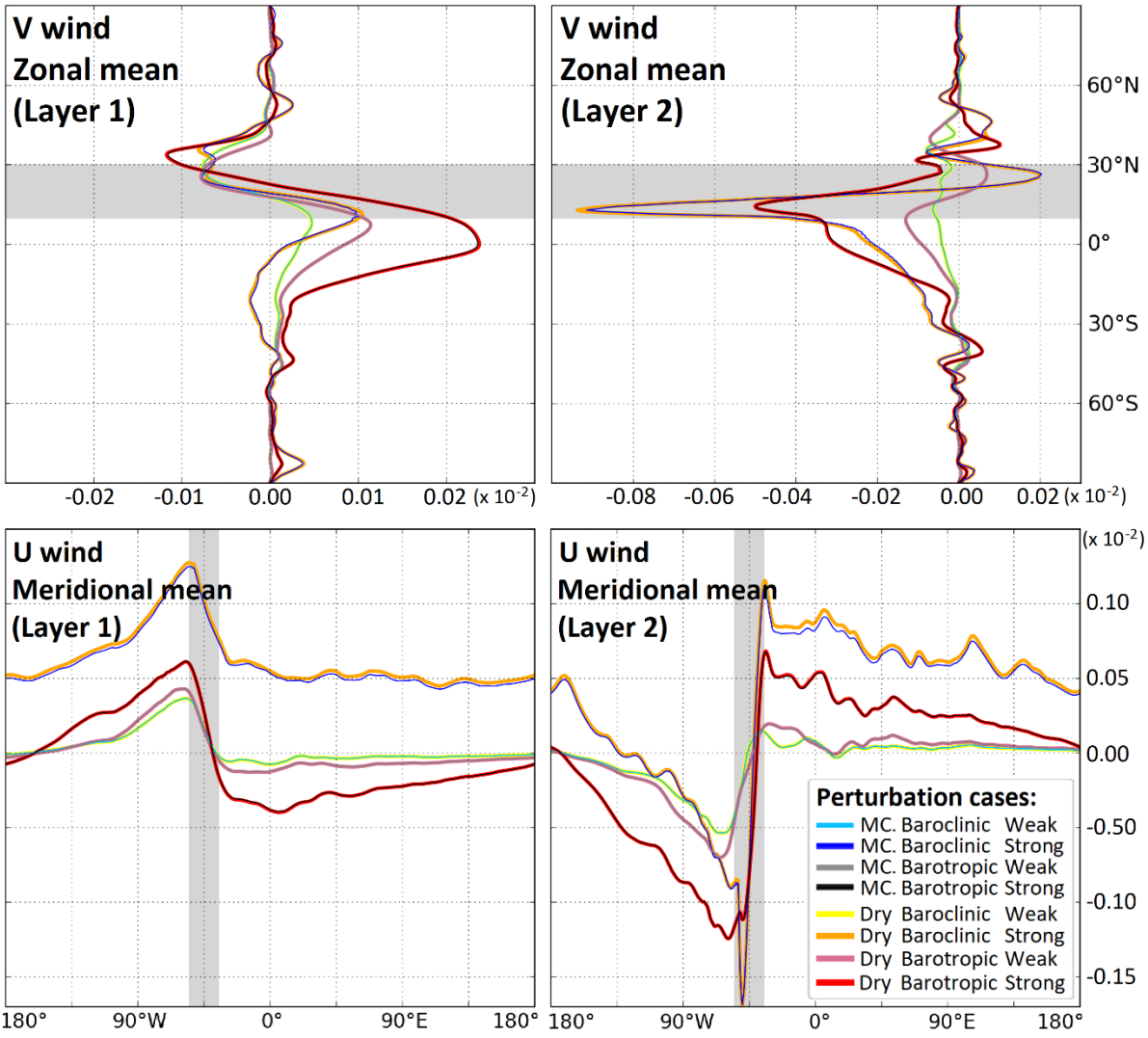

Figure S11: Wind anomaly time-mean relative to the reference case, for moist-convective (MC) and dry situations. The gray shade represents the initial buoyancy perturbation region.

References

1. Burns, K. J., Vasil, G. M., Oishi, J. S., Lecoanet, D., Brown, B. P. Dedalus: A Flexible Framework for Numerical Simulations with Spectral Methods. *Physical Review Research*, **2**, 2. DOI: 10.1103/PhysRevResearch.2.023068 (2020).

2. Cao, Y., Kurganov, A., Liu, Y., Zeitlin, V. Flux globalization based well-balanced path-conservative central upwind scheme for two-layer thermal rotating shallow water equations. *Journal of Computational Physics*, **474**, 111790. DOI: 10.1016/j.jcp.2022.111790 (2023).

3. Cao, Y., Kurganov, A., Liu, Y., Zeitlin, V. Flux globalization-based well-balanced path-conservative central-upwind scheme for two-dimensional two-layer thermal rotating shallow water equations. *Journal of Computational Physics*, **515**, 113273. DOI: 10.1016/j.jcp.2024.113273 (2024).

4. Cao, Y., Kurganov, A., Liu, Y., Rostami, M., Zeitlin, V. On the dynamics of equatorial excited dipolar systems. *Physics of Fluids*, **37** (5), 056618. DOI: 10.1063/5.0270628 (2025).

5. Castro, M. J., LeFloch, P. G., Muñoz-Ruiz, M. L., Parés, C. Why many theories of shock waves are necessary: Convergence error in formally path-consistent schemes. *Journal of Computational Physics*, **227** (17), 8107–8129. DOI: 10.1016/j.jcp.2008.05.012 (2008).

6. Castro, M. J., Luna, T. M., Parés, C. Well-balanced schemes and path-conservative numerical methods. *Handbook of Numerical Methods for Hyperbolic Problems, Elsevier*, **18**, pp.131–175. DOI: 10.1016/bs.hna.2016.10.002 (2017).

7. LeFloch, P. G. Hyperbolic Systems of Conservation Laws: The Theory of Classical and Nonclassical Shock Waves. *ASME Applied Mechanics Reviews*, **56** (4), B53–B54. DOI: 10.1115/1.1579455 (2003).

8. Maso, G. D., Floch, P. L., Murat, F. Definition and weak stability of nonconservative products. *Journal de Mathématiques Pures et Appliquées*, **74**, 483-548. Source: zbmath.org/0853.35068 (1995).

9. Parés, C. Numerical methods for nonconservative hyperbolic systems: A theoretical framework. *SIAM Journal on Numerical Analysis*. **44** (1), 300–321. DOI: 10.1137/050628052 (2006).

10. Parés, C. Path-conservative numerical methods for nonconservative hyperbolic systems. *Numerical Methods for Balance Laws, Quaderni di Matematica*, **24**, pp. 67–121. Source: zbmath.org/1266.65148 (2009).

11. Rostami, M., Petri, S., Guimarães, S.O., Fallah, B. Open-source stand-alone version of atmosphere model Aeolus 2.0 Software. *Geoscience Data Journal*, **11**, 1086–1093. DOI: 10.1002/gdj3.249 (2024).

12. Rostami, M., Petri, S., Fallah, B., Fazel-Rastgar, F. Aeolus 2.0's thermal rotating shallow water model: A new paradigm for simulating extreme heatwaves, westerly jet intensification, and more. *Physics of Fluids*, **37** (1), 016604. DOI: 10.1063/5.0244908 (2025).